Applied Physics A (2025) 131:62
https://doi.org/10.1007/s00339-024-08157-4

Applied Physics A
Materials Science & Processing

S.I. : SR2A - SYNCHROTRON RADIATION AND NEUTRONS IN ART AND ARCHAEOLOGY 2023

Application of scanning small-angle X-ray scattering in the identification of sheet formation techniques in historical papers

Małgorzata Grzelec[1] · **Sylvio Haas**[2] · **Agnieszka Helman-Ważny**[1,3,4]

Received: 2 August 2024 / Accepted: 3 December 2024 / Published online: 24 December 2024

Abstract
Among writing substrates produced historically in different regions of the world, paper is one of the most complex materials. Its complexity results not only from a variety of highly processed ingredients, which can be used in its production, but also from a variety of methods in which these materials are combined to form the fibrillar network referred to as paper. While material identification methods are well established in the analysis of historical papers, the identification of manufacturing technologies is still an under-researched topic, that requires the development of appropriate methods and measurement protocols. This paper reports on the results of a research project aimed at the application of synchrotron scanning small angle X-ray scattering (SAXS) method in the characterization of paper structure, with emphasis on the assessment of fibrillar orientation as a marker characteristic for different, historical papermaking technologies. The main objective of this study consists of the development of a measurement protocol involving the SAXS technique complemented by other analytical methods in the characterization of the fibrous paper structure.

Keywords SAXS · Fiber orientation · Paper analysis · Papermaking technology

1 Paper structure and its relationship to papermaking technology

Paper structure is often described based on a model of hierarchical organization. In this model, the most fundamental level of paper organization is the molecular level, where among different compounds present in the plant fiber used in paper manufacturing, cellulose, hemicelluloses, and lignin define the structure and properties of paper. The dimensions of these polymeric elements range from 1–10 nm and provide information on fiber chemical composition, degree of crystallinity, crystal structure, or molecular weight [1]. At a higher level of organization, these polymers aggregate to form the fundamental building blocks of fibrillar matter. These basic units are intermittently referred to as microfibrils, microfibers, nanofibrils, or nanofibers, to describe fibrous material at a scale between 4 nm and a few hundred nanometers [2]. The structural organization within a single nanofibril consists of more orderly positioned cellulose chains bound by a matrix of amorphous material, composed of hemicelluloses and lignin [5], and is characteristic for plant species [6]. Upon aggregation, microfibrils form individual cells of diameter between 7 to 50 µm [4]. Plant cells comprise various types of elements, the most abundant of which are fibers. Typically, the alignment of cellulose chains in a single fiber follows random orientation in the primary wall layer, and helical orientation in the secondary wall layers [5]. Aligned cellulose nanofibrils are bound by the amorphous matrix composed of hemicelluloses and lignin.

Most papermaking plant fibers belong to sclerenchyma cells, except for cotton, whose fibers are classified as elongated epidermal cells [4]. The fibers used to produce paper are sourced from different parts of plants, and based on the source divided into groups of bast fibers, grass fibers, wood fibers, leaf fibers, and fruit fibers [7]. The individual fibers

✉ Małgorzata Grzelec
malgorzata.grzelec@uni-hamburg.de

1 Centre for the Study of Manuscript Cultures (CSMC), University of Hamburg, Hamburg, Germany

2 Deutsches Elektronen-Synchrotron (DESY), Hamburg, Germany

3 Bundesanstalt Für Materialforschung Und -Prüfung (BAM), Berlin, Germany

4 University of Warsaw, Warsaw, Poland

vary in anatomical characteristics, which are the basis for their identification, such as shape of fibers, thickness, length, width of cell wall, width of lumen, cross-markings, longitudinal striation, fiber twist, shape of fiber ends, and presence of knots and joints. Except for fibers, the majority of plant material used in papermaking exhibits the presence of other types of cells, such as, among others, tracheids, parenchyma, vessels, epidermal cells, epidermal hairs, as well as accompanying mineral material such as crystals and silica bodies (phytholiths), which help in differentiation of plant species [7].

In the traditional papermaking process, the fibrous plant material is altered at multiple structural levels, beginning from the molecular and nanofibrillar levels. The initial stages after fiber sourcing consist of treatments aimed at increasing the bonding surface between the fibrillar matter during paper sheet formation. Among different forces, the primary bonding mechanisms are the oxygen–hydrogen bond linkage between cellulose and hemicelluloses in adjacent nanofibrils, as well as van der Walls forces. To increase the number of bonding sites the fibers are processed to disintegrate the lignocellulosic structure by removing the lignin and part of hemicelluloses fraction and loosen up the cellulosic matter by chemical and mechanical methods. Historically, chemical methods involved cooking fibrous material with the addition of alkali such as wood potash or lime [8, 9] (Fig. 1 a). Alkaline treatment damages hydrocarbon–lignin linkages which facilitates subsequent lignin removal through rinsing. In the alkaline cooking process, the cell's primary wall is oftentimes partly or completely removed, as it contains a significant amount of lignin. Except for the removal of the non-cellulosic fractions, the treatment softens the remainder of fibrous matter, which in turn allows for easier processing during the next stage, involving beating. Before industrialization, the wet fibers were traditionally beaten by hand with wooden mallets and paddles (Fig. 1b). Beating leads to displacement, deformation, breaking of cell walls, and swelling which in turn enables gradual external and internal fibrillation, a process in which the fiber is split longitudinally into fine fibrils that remain attached to the fiber. The fibrillated fibers absorb water, whose molecules perform an important function in forming hydrogen bonds between fibrils during sheet formation and drying process [10]. These processing steps are reflected in structural changes of the fibers such as wall dislocations and fractures, deformations in crystalline structure in the form of slip planes, regions of localized delamination in the fiber, and compressive strain in the form of nodes, micro-compressions, kinks, and ballooning resulting from the activity of swelling agents [11]. To form a paper sheet, first, the papermaking slurry consisting of processed fibers is prepared by evenly distributing pulped fibers in a water-filled vat by stirring. Next, the fibers are deposited onto a papermaking sieve mounted on a wooden frame referred to as papermaking mold, by submerging the mold in the water (Fig. 1 c). Different submerging techniques are discussed in detail in the following paragraphs.

1.1 Fiber parameters influencing distribution and orientation

Two main fiber parameters influencing the distribution of fibers within paper sheets can be distinguished. These include fiber length and fiber coarseness. Fiber length is the most important factor. Greater fiber length leads to increased flocculation—the formation of big flocks of fibers—which results in decreased uniformity of fiber distribution. In effect, the formed paper sheet shows spotty areas of greater and lower density and thickness [12, 13] (Fig. 2). Pulp consisting of only short fibers, on the other hand, yields papers more uniform because shorter fibers show decreased fiber contact (crowding factor) [14], but are also mechanically less resistant [15]. The most optimum papermaking slurry is composed of both longer and shorter fibers, produced in the process of cutting and beating. This way the long fibers form a primary net structure, that is subsequently filled in with shortened fibers [16].

The next significant factor is fiber coarseness, which is a measure of rigidity of the fiber, resulting from the thickness of its secondary wall. The thinner the wall, the easier the fiber collapses upon drying and the flatter it becomes. The

Fig. 1 Selected stages of the traditional papermaking process: Cooking plant fibers in an alkaline solution to remove non-cellulosic fractions and improve fiber bonding (**a**) manual beating of the fibers with a wooden mallet to further loosen the fibrillar fiber structure (**b**), and sheet formation by scooping of the diluted pulp from a vat, using papermaking mold equipped with a bamboo sieve (**c**). Fot. Małgorzata Grzelec

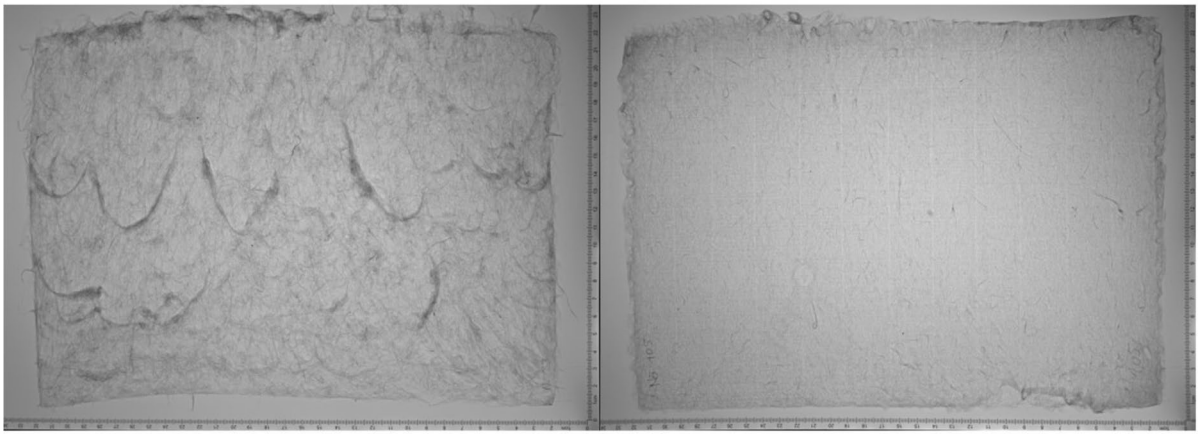

Fig. 2 Transmissive light images of a sheet manufactured by the scooping method from paper mulberry fibers. The sheet without the addition of formation aid (left) shows areas of flocculated fibers in the direction of the propagation of the paper slurry liquid. The sheet with the addition of formation aid (right) shows more uniform distribution, without visible flocs, fot. Małgorzata Grzelec

collapse of cell walls results in denser pulp, with shorter inter-fiber distances. Additionally, the coarser the fiber, the more likely it is to form flocks [12]. One of the secondary properties of fibers that may influence sheet formation is their chemical composition, which can impact the efficiency of dewatering. Fibers sourced from different parts of the plant may differ in chemical constituents and structure and retain water to a different degree [17]. Extended water draining time increases the difference in fiber orientation anisotropy between the sieve side and the top side [18].

Other factors influencing fiber distribution and orientation are related to the fiber processing techniques. Pulp consistency is one of these parameters, and it is adjusted by the papermaker before and in the course of the sheet formation process. Pulp consistency is defined as the ratio of the weight of dry fiber mass to the weight of the papermaking slurry sample. Papermakers opt for pulp consistencies between 0.1 to 1%, and to be kept constant the concentration of the pulp has to be adjusted with the formation of consecutive paper sheets, by adding fibers as the slurry becomes gradually more diluted. Upon increasing pulp consistency, the fibers tend to flocculate more, until a point of saturation, after which the tendency to flocculate starts to decrease again [12]. The degree of fibrillation is another important technological parameter, which influences the distribution of fibers. Highly fibrillated pulp tends to retain more water, both due to increased surface area resulting from internal and external fibrillation and the presence of cellulosic fines, as well as the tendency of the fines to clog the inter-fiber spaces, which prevents water from draining [19].

To improve fiber distribution a formation aid can be added to the papermaking slurry. Historically, natural mucilages would be used as formation aids, sourced from plants such as aloe vera or hibiscus roots [20]. The presence of formation aid increases pulp viscosity, decreases the tendency of fibers to flocculate, and slows down water drainage [12] (Fig. 2).

1.2 Relationship of sheet formation techniques and fiber orientation

The process of sheet formation has been researched for industrial papermaking [21–23], but the mechanisms governing the process within traditional methods have not been described so far. Based on observations of the work performed by contemporary practitioners within these traditional papermaking technologies, as well as the analysis of technological features of papers manufactured by these methods, it is proposed that the process of depositing fibers on the papermaking sieve involves a method-dependent interplay of different hydrodynamic forces and fiber-fiber interactions. The general principle of fiber deposition on the sieve involves the movement of the fibers along the flow direction of the fluid counteracted by the gravitational force of the draining water. Depending on the sheet formation method shearing conditions may differ and involve the complex differential contributions of laminar and turbulent flow. The contribution of different types of flow allows fibers to be distributed evenly and avoid the formation of flocs [24]. The type of flow present can be modeled based on the principle behind the Reynolds number, defined as the ratio of the velocity of the fluid times the length of the fiber over the viscosity of the fluid. If the magnitude of inertia is greater than viscosity, turbulent flow can arise. If viscosity is greater, the resulting flow is laminar.

Multitude variations of sheet formation techniques have been identified in different geographical regions. The papermaking mold is used to deposit fibers on a sieve in a fine

layer. The process can involve different forms of the mold, which evolved based on differing fiber depositing techniques. In the European papermaking tradition, the mold is built of metal wire mesh attached to a wooden frame, arranged in a regular pattern of so-called laid lines which was used to manufacture laid paper, or inlaid with a piece of wire—cloth, that resulted in production of so-called wove paper. In European papermaking, the sheet formation process involved dipping the mold in the papermaking slurry, which was subsequently rapidly pulled out and vigorously shaken to facilitate water drainage (Fig. 3) [https://lecture2go.uni-hamburg.de/l2go/-/get/v/69784]. Notably, in East Asian papermaking a similar method, *tamezuki*, was developed as well and consists in single dipping of the sieve in the vat.

In the Japanese or Korean papermaking traditions, the papermaking mold would consist of a wooden frame and a bamboo sieve. Mostly laid—type papers were produced with this method. The most prevalent East Asian sheet formation method is usually referred to as *nagashi-zuki*, or scooping method. In this method the fibers were scooped from the papermaking vat with single or bi-directional, wide, sweeping motions of the mold, often suspended on a cord to assist in swinging (Fig. 3) [https://lecture2go.uni-hamburg.de/l2go/-/get/v/69786]. In this method addition of formation aid, increasing the viscosity of the fluid, is critical to produce laminar flow and achieve even distribution of the fibers.

The other, distinctive sheet formation technique, widespread in Highland Asia, in regions such as Nepal or Tibet, is the pouring method, often requiring the use of a floating mold [25]. The wooden frame is equipped with a textile mesh, so within these papermaking traditions, mostly wove papers would be produced. The difference consists in how the fibers are deposited in the pouring method. In this technique, the mold is reversed top to bottom and placed in a tray shallowly filled with water, the thick papermaking slurry is poured on top of the sieve from a cup (Fig. 3) and manually distributed over the sieve [26] [https://lecture2go.uni-hamburg.de/l2go/-/get/v/69788].

Across these papermaking traditions the sieves of wove type, usually made of cotton, were developed to facilitate water drainage, speed up the process of paper production and increase durability of the end product. Generally, the finer the structure of the sieve, the better-quality paper can be produced, but at a cost of time efficiency. While both in the dipping and scooping method, the formed sheet of paper is removed from the mold while still moist, in the case of the pouring method with the floating mold the papermaker has to wait until the sheet is completely dry to be able to remove it.

The method of fiber deposition is often reflected in the pattern of fiber orientation within the entire sheet. Based on technological analysis it is proposed that paper sheets formed using the dipping method show greater orientation isotropy. Papers produced by pouring seem to exhibit more variability in terms of fiber orientation, as well as fiber distribution, showing areas of localized anisotropy, differences in density, and resulting differences in sheet thickness. In the case of scooping technique, the fibers are likely to exhibit characteristic dominant orientation along a specific direction (Fig. 4 b). Additionally, in all of the techniques, fiber orientation can be different for the sieve side and the top side of the paper sheet, which is related to differential fluid flow processes across the thickness of the fiber layer deposited on the sieve. Fibers in direct contact with the sieve mesh orient themselves instantly along the direction of water drainage, while fibers closer to the top surface of the sheet experience delayed onset of gravitational forces which results in prolonged freedom of movement leading to more random orientation (Fig. 4 a) [27, 28]. This side-specific orientation difference can be more prominent for certain sheet formation techniques and materials exhibiting longer dewatering times. Importantly, because the sheet formation techniques can be modified or combined, and because industrialization introduced partial mechanization into the papermaking processes in some regions, the fiber orientation patterns can show considerable variability.

.

Fig. 3 Three historical sheet formation methods; Dipping method (left): Fibers are deposited onto the sieve by a single dip of the papermaking mold into the vat, which is then immediately lifted. Scooping method (center): Also known as *nagashi-zuki*, where fibers are scooped with the mold and uniformly distributed on the sieve by swinging motions. Pouring method (right): The pulp is distributed by pouring the slurry from a cup onto a mold suspended in water. Fot. Małgorzata Grzelec

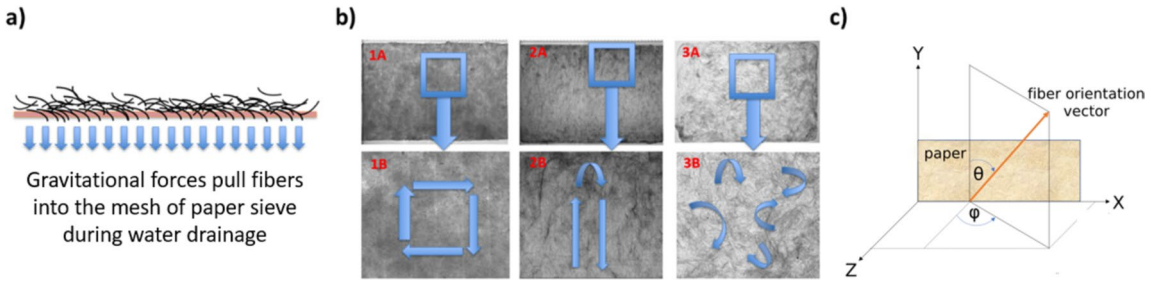

Fig. 4 **a** Sketch of gravity forces that align fibers. **b** The distribution of fibers within the sheet of paper reflects the movements of the mold or manual distribution of pulp on the sieve, depending on the sheet formation process; dipping method (1A,1B), scooping method (2A,2B), pouring method (3A,3B). **c** Coordinate system and definition of orientation angles

Assuming a three-dimensional structure of the paper sheet, where X and Y directions correspond to the width and height of the paper sheet ("in-plane" axes), and Z direction corresponds to the "out-of-plane" axis (Fig. 4 c), it is proposed that during sheet formation process the fibers align in specific patterns, related primarily to the sheet formation method, and to a lesser extent to the type of raw material. It is proposed that the differences in fluid flow vectors during sheet formation by dipping, scooping, and pouring account for the differences in fiber distribution and orientation. Methods of raw material and structure characterization were employed to characterize fiber identity, fiber network, fiber distribution, and orientation within three dimensions. To identify the type of raw material, optical and SEM microscopy were employed [29, 30]. SEM microscopy was used as well, alongside digital microscopy, to characterize fiber networks and image processing methods were used to extract information about in-plane fiber orientation from the digital microscopic images [27, 28, 31]. Scanning small-angle X-ray scattering was used to probe fibrillar orientation within the nanoscale [32], where the collected data accounts for three-dimensional fiber orientation.

2 Materials and methods

2.1 Sample preparation

Out of 40 measured samples, 20 contemporary, hand-made papers have been selected, to represent a variety of geographical origin, raw materials, and papermaking technologies (Table 1). The samples underwent SAXS and digital microscopy measurements first, and in the next stage, fibrous material was sourced for Light Microscopy and SEM. First, the samples selected from central areas of the paper sheets have been trimmed to the size required for mounting on custom-made holders installed at the SAXS stage, with the dimensions of each sample equal to 20 × 40 mm. The direction of the laid lines was noted and the thickness of each sample was measured with a digital micrometer. Next, a few milligrams of fibrous material were sampled from each paper type, boiled in deionized water to remove adhesives, dried and subsequently mounted on microscopic slides in Poly(butylmethacrylat-*co*-methylmethacrylat)—based mounting medium (Eukitt).

.

2.2 Optical microscopy

Images of fibers mounted in a mounting medium have been captured with Olympus BX51 optical microscope, equipped with Olympus TH4-200 light source, and 5 × and 10 × MPlan

Table 1 Types of fibers identified in the samples of hand-made papers

Geographical region	Number of samples	Fiber type	Fiber species	Manufacturing method
Europe	7	European bast, Fruit	*Linnum ussitassimum, Gossypium, Cannabis sativa*	Dipping
East Asia	5	Asian bast	*Borussonetia*	Scooping
Highland Asia	8	Asian bast	*Daphne bholua, Edgeworthia gardneri*	Pouring

N objectives. The images were captured in transmissive light mode and fiber measurements were performed by means of Olympus Stream 1.7 image analysis software.

2.3 Scanning electron microscopy

Fragments of approximately 2 × 2 mm dimensions were cut out and prepared by gold coating using a sputter coater. The deposited gold layer had a thickness of about 10 nm. The images were taken using a Field Emission Scanning Electron Microscope Quanta FEG 250 (ThermoFisherScientific (FEI)), at ultra-high vacuum of around 1.02e^-5 Pa. Images were collected at 600× and 10.000× magnifications.

2.4 Digital microscopy

Images of the paper samples were taken with Keyence VHX-5000 digital microscope, equipped with the VH-Z100UR objective. Photographs were captured at a 200× magnification setting, with full ring illumination in a 3D composition mode, where consecutive images were taken along the z-axis, at an automatic vertical pitch setting.

2.5 Image processing

Images captured with a digital microscope underwent image processing in ImageJ software, version 1.54 d, equipped with an OrientationJ plug-in, version 2.0.5 [33]. Images underwent rasterization to 8bpp bitmap files (Fig. 7 a, b), and subsequent orientation estimation (Fig. 7 c) based on the evaluation of local structure tensor (J, 1). The gradient was computed using the cubic spline method, where the standard deviation defining the local window was set to σ = 2 pixels. The resulting data represents orientation distribution (θ, 2) intensity across angles ranging from − 90° to 90°, where 0° denotes horizontal direction. Simultaneously, coherence (C, 3) value was calculated for each of the images, to assess the degree of anisotropy. Coherence is equal to 1 when the local structure has a dominant orientation and to 0 if the image is locally isotropic.

$$\mathrm{J} = \nabla f, \nabla f_w^T = \begin{bmatrix} f_x,f_{xw} & f_x,f_{yw} \\ f_x,f_{yw} & f_y,f_{yw} \end{bmatrix} \tag{1}$$

$$\theta = \frac{1}{2}\arctan\left(2\frac{f_x,f_{yw}}{f_y,f_y - f_x,f_{xw}}\right) \tag{2}$$

$$\mathrm{C} = \frac{\lambda_{max} - \lambda_{min}}{\lambda_{max} + \lambda_{min}} = \frac{\left(f_y,f_{yw} - f_x,f_{xw}\right) + 4f_x,f_{yw}}{f_x,f_{xw} + f_y,f_{yw}}, \mathrm{C}\varepsilon[0..1] \tag{3}$$

2.6 Small angle X-ray scattering

SAXS measurements were performed at the SAXS-MAT beamline P62 [34], at the DESY facility in Hamburg, Germany. A wavelength of 1 Å and a beam size of 200 × 200 μm^2 has been used. The samples were mounted on a custom-made 3D-printed sample holder, allowing for sample rotation with respect to the incoming beam. An area of 15 × 15 mm^2 with a step size of 250 μm has been raster scanned. For each sample, the area was scanned at 4 angles of inclination ω= 0°, 30°, 45° and 60° with respect to the incoming beam. The exposure time per point was 200 ms to ensure a low X-ray dose. It has been shown that an X-ray dose below 250 Gy–500 Gy will not cause radiation damage to historical papers [35]. The exact value depends strongly on the paper and how it has been modified. Therefore, during the raster SAXS experiment the exposure time at each step was 200 ms which corresponds to an effective dose of roughly 25 Gy at 12.4 keV X-ray energy.

The SAXS patterns have been sector vice χ azimuthally averaged using the pyFAI package [36]. Each azimuthal sector covers 4° of angle. The covered q-range is 0.06–4.50 nm^{-1}. The determination of the main fibril orientation follows the method described by Georgiadis [37]. As a first step the χ_{max} of the maximum intensity at a $q = 0.2$ nm^{-1} as function of ω has been determined. The relation between (χ, ω) and the fibril orientation angles (θ, ϕ) is given by the following equation:

$$\tan(\chi) = \frac{\sin(\phi)\sin(\phi + \omega)}{\cos(\theta)} = \tan(\theta)\sin(\phi + \omega) \tag{4}$$

A least square fit implemented in MATLAB was used to fit Eq. 4 to the obtained $(\chi, \omega) - pairs$ to derive the fibril orientation angles θ and ϕ.

3 Results

3.1 Optical microscopy

Optical microscopy used in plant species identification allowed to obtain qualitative and quantitative information on the composition of the samples. Out of 20 samples, 18 contain only one type of raw material and the remaining two are composed of a mixture of fibers (Table 1). Within the sample group all of the papers, except for sample nr 5, comprise bast fibers of either European or Asian origin, including hemp (*Cannabis sativa*), flax (*Linum ussitassimum),* paper mulberry *(Broussonetia),* Lokta (*Daphne bholua)*, Argeli (*Edgeworthia gardneri*). Within the group of European papers cotton (*Gossypium*) fibers, belonging

to fruit type, were identified in sample nr 5. Samples nr 4 and 6 contain a mixture of bast fiber materials; flax and hemp mixed in different ratios.

Fiber species were identified based on their characteristic morphological features. European bast fibers, such as hemp, show the presence of multiple dislocations and cross–markings, as well as tapering blunt ends (Fig. 5 b). Occasionally wider, thin-walled fibers with axial pits or bundles of pitted fibers were also identified. The state of processing of the bast fibers in European paper samples reveals a characteristic, high degree of fibrillation; sample nr 7 presents the greatest degree of processing, visible as more areas of internal and external fibrillation, as well as fiber rupture, with characteristic fan-shaped fraying. The width measurements reveal that the fibers in the European bast fiber group are wider ($\bar{x} = 18.61$ um) and exhibit greater width deviation (RSD = 58.02%) than Asian bast fibers identified in the sample group ($\bar{x} = 10.67$um, RSD = 22.31%). An example of Asian bast material are Lokta fibers present in sample nr 25, showing presence of narrow fibers, which form bundles characterized by rigid bending. The fiber ends in *Daphne* species show a wide variety of shapes (Fig. 5 d), such as rounded, blunt, or forked.

Broussonetia fibers are identified based on the characteristic curvature of fiber bundles, and the presence of primary wall (transparent membrane, enveloping some of the fibers). An example constitutes the material sourced from sample nr 2 (Fig. 5 c).

Fruit fibers, such as in sample nr 5, containing *Gossypium* pulp, can be identified based on characteristic ribbon-like twisting (Fig. 5a), surface smoothness, and the presence of broken-off ends at the base of individual fibers (Fig 5).

3.2 Scanning Electron Microscopy

Observation of the fibers performed at 600× magnification allows the characterization of the fiber network within each of the paper samples, while at 10.000× magnification allows for inspecting the surface microstructure of individual fibers.

The long *Broussonetia* fibers in sample nr 3 (Fig. 6 a, b) form a net intertwined with abundant extracellular matter. Characteristic elements of membrane enveloping individual fibers, partly detached in the beating process are visible in some areas of the fiber network. At 10.000× magnification, the smoothness of the individual mulberry fibers is well visible, as well as their relative coarseness. Compared with the next sample, nr 5, containing *Gossypium* pulp (Fig. 6 c, d), the fibers are less flattened and show much less fibrillation.

Cotton fibers in sample nr 5 are wider and flat, occasionally exhibiting a curved profile and the characteristic ribbon-like twisting. The fibrous network shows a significant degree of fibrillation, resulting in an irregular web of microfibrillar bridges. At a magnification the individual fiber's surface shows the presence of microfibrils with a helical twist.

SEM images of *Cannabis sativa* fibers in sample nr 7 reveal a high degree of fibrillation (Fig. 6 e, f). The resulting, increased bonding area leads to fibers more tightly

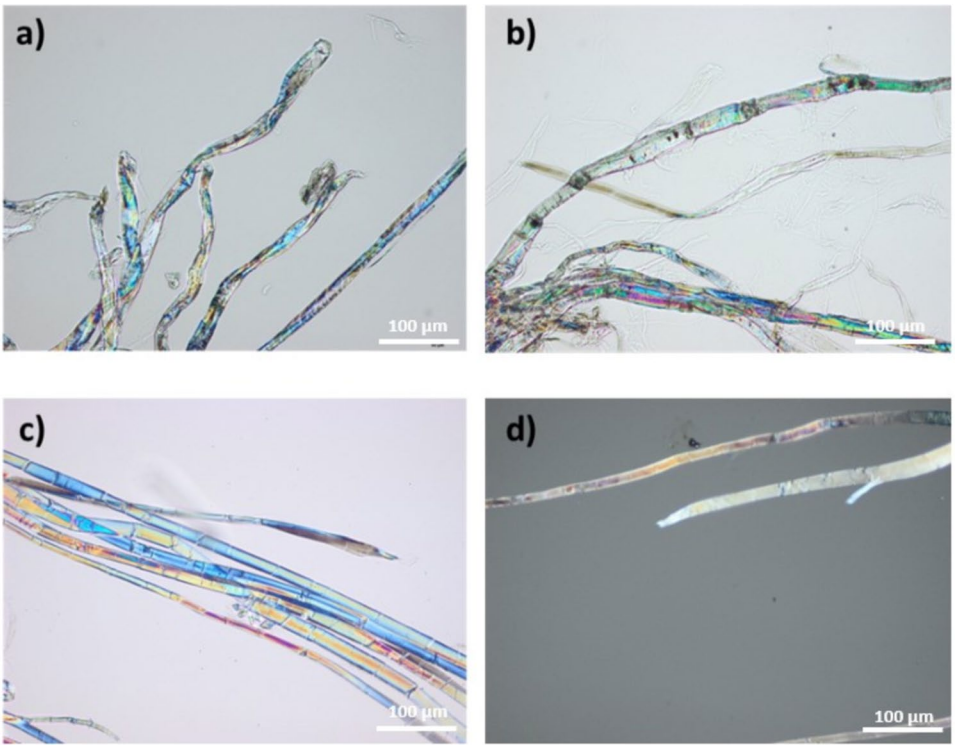

Fig. 5 **a** Cotton fibers, sample nr 5, showing ribbon-like twist **b** Hemp fibers, sample nr 7, presenting multiple dislocations **c** Paper mulberry fibers, sample nr 20, forming a curved bundle **d** Daphne fibers, sample nr 25, with characteristic fiber ends. The magnification was ×20 for all images and cross-polarized light was used

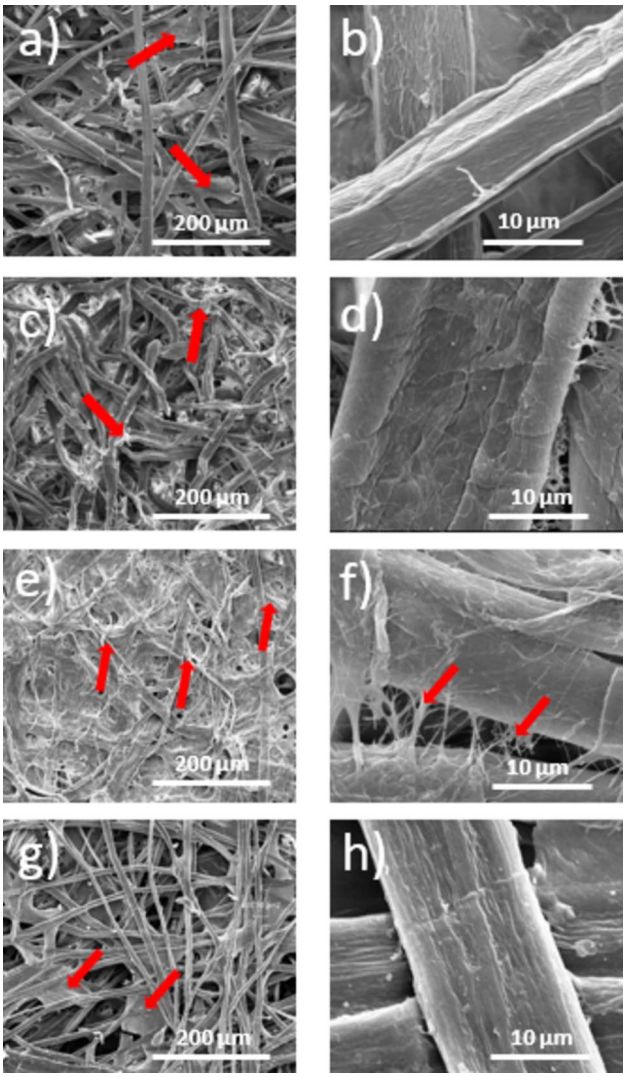

Fig. 6 Sample nr 2, Borussonetia fibers at 600× magnification showing regions of amorphous matter between the fibers (red arrows) (**a**), and at 10.000× magnification showing coarseness of the fiber (**b**). Sample nr 5, Gossypium fibers at 600× magnification, with visible ribbon-like twisting and regions of fibrillation (red arrows) (**c**), and at 10.000× magnification with visible flat and concave form of a single fiber (**d**). Sample nr 7, Cannabis sativa fibers at 600× and 10.000× magnification, showing high degree of fibrillation (red arrows) (**e**, **f**). Sample nr 25, Daphne fibers, at 600× and 10.000× magnification showing smooth surface and presence of inter-fiber amorphous matter (red arrows) (**g**, **h**)

bound together, with visibly less inter-fiber spaces. At a 10.000× magnification, the characteristics of the surface structure of the fibers become more prominent; notably fine microfibrillar bridges connecting the individual fibers and the irregular fiber surface texture, with splitting of the fine fibrillar material, and jagged fiber ends.

SEM images of sample nr 25 reveal an arrangement of smooth, narrow interlocking fibers characteristic of *Daphne* genus (Fig. 6 g, h), with abundant amorphous substances connecting individual fibers. At a 10.000× magnification fibers' surface is mostly visibly intact, without markers of fibrillation.

3.3 Digital microscopy and image processing for fiber orientation in-plane

The results of surface imaging with a digital microscope reveal information about the in-plane orientation of fibers with respect to the paper sheet side. The relative intensity of fiber orientation across the angle range was plotted as colormaps, where orientation angles with greatest intensity are colored red and lowest intensity are colored blue (Fig. 7 c). Majority of the samples in the group of papers produced by dipping method shows bilaterally similar orientation with maximum average intensity at 83.86° ($\sigma = 4.50$). In the case of papers manufactured by pouring, the dominant orientation direction ($\bar{x} = 67.81$) shows more variability spanning a wide range of angle values ($\sigma = 29.99$). The group of papers produced by scooping shows similarly high dominant orientation variability, where orientation within 80–90 ° and 0–10 ° are most common ($\bar{x} = 44.70$, $\sigma = 37.43$). Comparison of coherence values reveals information about the degree of anisotropy for each side of individual samples, as well as for samples compared to one another. The coherence values calculated for two sides of each sample underwent analysis of variance ANOVA to understand whether significant differences can be observed between groups of samples manufactured by different sheet formation methods. The differences between groups are statistically significant ($p = 0.0056$, $F = 5.98$). The samples with the greatest differences in side-specific coherence values belong to the group of papers manufactured by the pouring ($\sigma = 0.037$) and scooping methods ($\sigma = 0.037$). The samples with the lowest deviation of coherence values represent the dipping method ($\sigma = 0.017$). Samples produced by scooping show the highest average coherence value ($\bar{x} = 0.091$), followed by samples manufactured by pouring ($\bar{x} = 0.070$) and dipping method ($\bar{x} = 0.047$).

3.4 Fibrillar orientation measured with SAXS

Analysis of fibrillar orientation with SAXS allows for identifying the alignment in the out-of-plane direction. Orientation information has been collected for the entire scan area for each sample. Hereby, the orientation angles θ and φ in real space coordinate system were determined using Eq. 4. The orientation along polar angle θ and azimuthal angle φ is visualized as colormaps of the scanned area, as well as probability density of orientation along each angle range are exemplary shown for sample 7 (Fig. 8), sample 2 (Fig. 9) and sample 23 (Fig. 10). To allow for easier identification of dominant modes in the orientation distribution of each

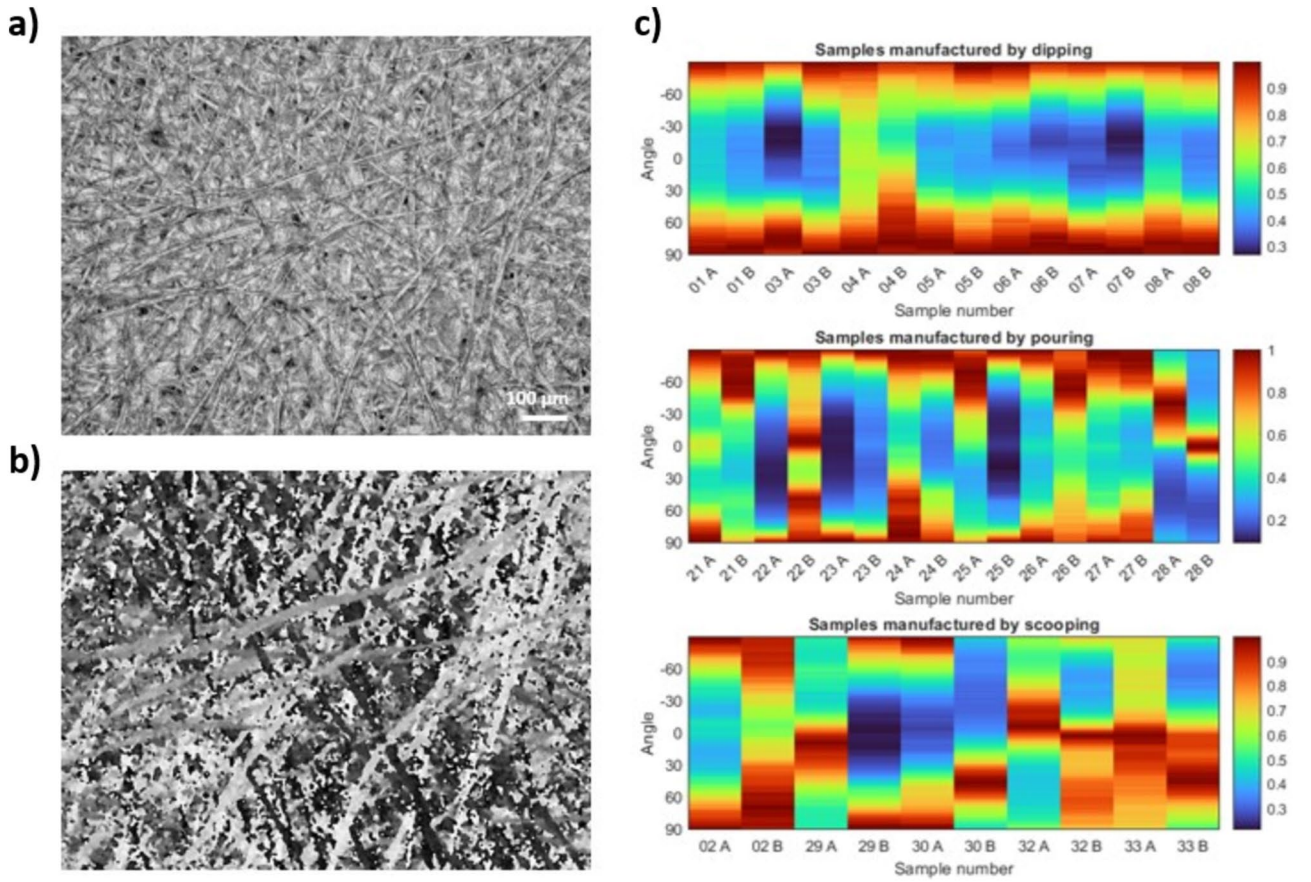

Fig. 7 Digital microscope images (**a**) underwent image processing for edge detection (**b**) and the obtained orientation information was presented as colormaps for samples manufactured by dipping, pouring and scooping (**c**)

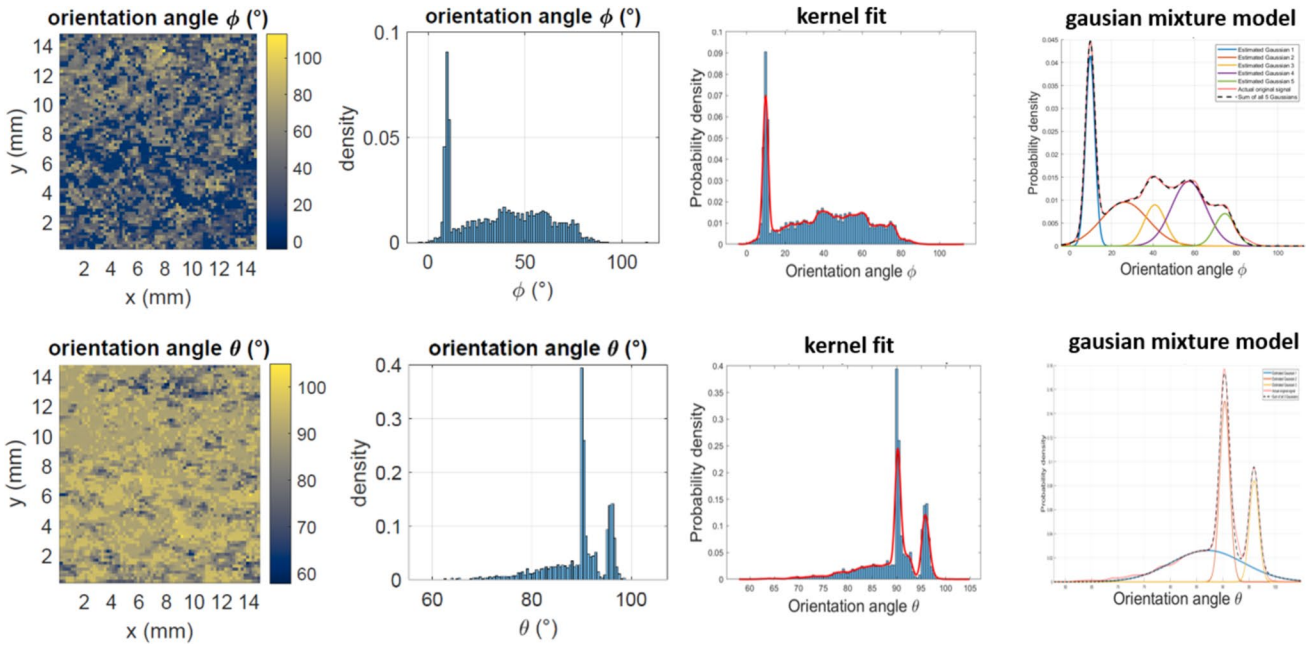

Fig. 8 Orientation distribution maps, probability density histograms, kernel fit graphs and Gaussian Mixture Model graphs for sample no. 7, upper line: results for azimuthal angle φ; lower line: results for polar angle θ

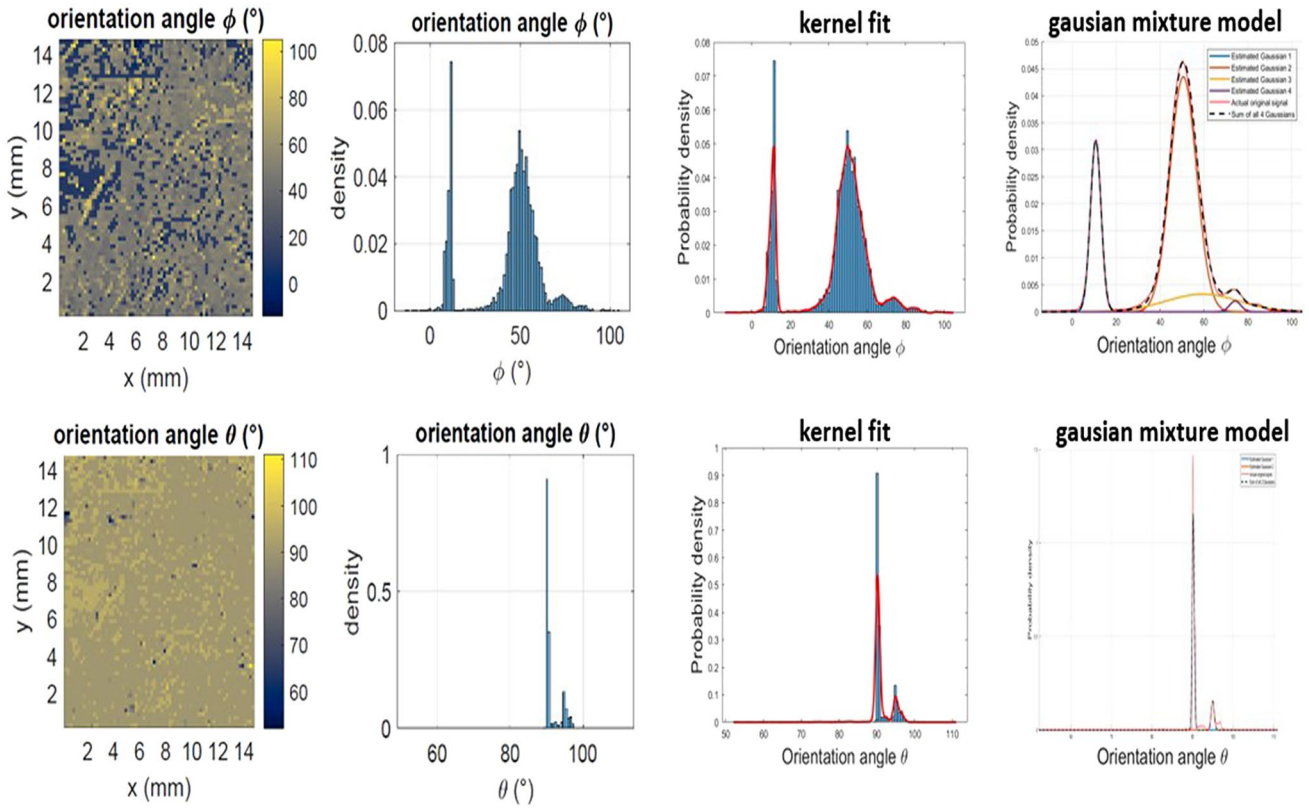

Fig. 9 Orientation distribution maps, probability density histograms, kernel fit graphs and Gaussian Mixture Model graphs for sample no. 2, upper line: results for azimuthal angle φ; lower line: results for polar angle θ

scanned sample, the kernel function was fitted to all distribution plots, which were subsequently deconvoluted by fitting Gaussian Mixture Models. To avoid overfitting, the best fits were chosen based on the comparison of minimum mean residual values with results of Bayesian Information Criterion estimation for each distribution. The weight of each Gaussian, expressed in %, was calculated as a fraction of the area under the kernel function curve. The positions of Gaussian peaks and their weights for all of the samples have been listed in the tables, and grouped according to the sheet formation technique (Table 2, 3).

In comparison, the total number of modes identified in each distribution plot for φ angle is higher for samples manufactured by the pouring method (5.25 modes/sample) and by the dipping method (5.14 modes/sample), than for samples produced by the scooping method (4.80 modes/sample). For all three sample groups, the peaks located between 40 to 60 ° φ constitute the dominant peaks and contribute on average about 51.9% (dipped), 57.5% (poured), and 73.7% (scooped) of orientation distribution. Modes between 0 to 40 ° φ contribute on average 19.2% of orientation in papers manufactured by scooping, 28.9% in samples produced by pouring, and 34.9% of distribution in samples produced by dipping. Angle range above 60 ° φ in the group of dipped samples contributed only about 1.7% of orientation distribution, while a significantly higher ratio was recorded for scooped (11.3%) and poured samples (13.5%).

For orientation distribution along angle θ the samples within all three groups show characteristic dominant, tall peaks around 90 ° that account for the majority of the distribution. The second, short peak at around 95 ° contributes to the distribution to a varying degree, with 16.4% for scooped samples, 19.9% for dipped samples, and 20.2% for poured samples.

Another characteristic feature differentiating the groups of samples is the presence of a broad peak or tailing of the distribution below 90°. Compared to scooped and poured paper samples the group of samples produced by the dipping method shows a considerably greater portion of the distribution spanning below 90° as far as 40–60° for 5 out of 7 samples.

To enable comparison of different types of probability distributions present across the sample set, Jensen—Shannon divergence was used to measure the pairwise distances between all of the distributions. Jensen—Shannon divergence is bounded between [0,1], where 0 indicates identical probabilities and 1 indicates that they are completely different. Heatmaps for divergence scores were plotted for

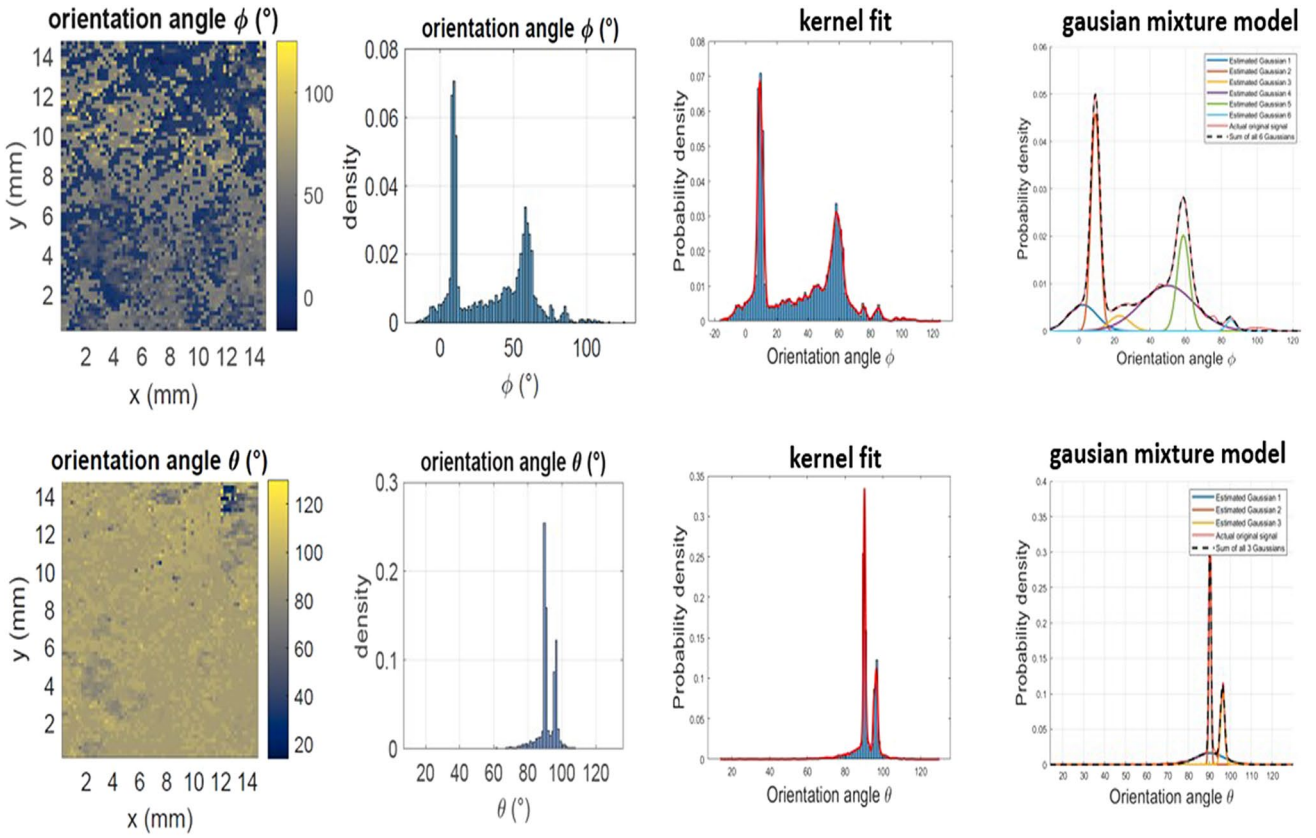

Fig. 10 Orientation distribution maps, probability density histograms, kernel fit graphs and Gaussian Mixture Model graphs for sample no. 23, upper line: results for azimuthal angle φ; lower line: results for polar angle θ

both φ and θ distribution datasets (Fig. 11, 12). The heatmap for distribution along φ reveals a degree of similarity between samples manufactured by the dipping method, followed by the group of samples produced by scooping. The samples obtained by the pouring method do not show significant pair-wise similarity within the group. Some of the samples from different groups of poured and scooped papers show a degree of pair-wise similarity as well. In the case of heatmap for distribution along θ angle, none of the sample groups show a significant degree of in-group similarity. The papers manufactured by the scooping method seem to be characterized by considerably dissimilar distributions not only in regards to samples from other groups but also within the group.

4 Conclusions and discussion

4.1 Fiber identification

Results of the microscopic identification of fibers in each of the paper groups revealed consistent use of the same plant species in each of the groups. Most of the papers manufactured by dipping contained bast fibers such as hemp or flax, with the exception of cotton in sample nr 5. All of the samples reveal a high degree of fibrillation and shortening of the fibers, which indicates an intense beating process. The type of raw material and processing used is historically accurate and constitutes a prerequisite for successful fiber deposition by dipping method. Similarly, Lokta and Argeli fibers identified in the group of samples manufactured by pouring are in accordance with the type of raw material used in this production method. These samples were collected by AHW in different parts of the Highland Asia region and constitute classical examples of the papers manufactured by pouring. Samples of the papers manufactured by scooping belong to species of paper mulberry, which have been commonly used in papermaking technologies involving the scooping sheet formation method. The degree of processing, compared to fibers in the dipping group, is significantly smaller, which is in accordance with the requirements for the method. The optimal fibers used in the scooping method are typically longer and the slurry is formed with the addition of natural mucilage as a formation aid, which ensures uniform fiber distribution.

Table 2 Comparison of data for fiber orientation distribution of individual samples along azimuthal angle φ. For consecutive peaks in each sample, values of the peak positions' maxima are represented in the first column and their weights are represented in the second column. Weight (%) denotes the ratio of the area of a peak to the area under the kernel fit curve

Name	Φ Peak 1	Weight (%)	Φ Peak 2	Weight(%)	Φ Peak 3	Weight(%)	Φ Peak 4	Weight(%)	Φ Peak 5	Weight(%)	Φ Peak 6	Weight(%)
S_01	10,08	9	31,06	13	43,88	24	56,75	38	71,05	16	–	–
S_03	10,14	7	35,06	18	45,45	28	57,04	25	70,04	22	–	–
S_04	10,08	27	13,67	16	42,42	26	58,17	14	71,94	14	87,12	2
S_05	10,07	14	22,66	7	42,12	37	58,53	28	72,40	13	–	–
S_06	9,25	26	19,54	11	51,48	29	59,45	25	75,21	8	–	–
S_07	9,75	23	26,29	27	40,85	12	57,15	29	74,52	9	–	–
S_08	9,50	40	22,21	7	48,91	26	58,43	21	74,13	6	–	–
Name	Φ Peak 1	Weight (%)	Φ Peak 2	Weight (%)	Φ Peak 3	Weight (%)	Φ Peak 4	Weight (%)	Φ Peak 5	Weight (%)	Φ Peak 6	Weight (%)
S_21	10,95	11	45,52	38	55,52	49	74,73	2	–	–	–	–
S_22	− 0,61	4	9,74	21	29,89	14	69,44	13	53,17	40	59,83	9
S_23	2,26	11	9,35	29	22,82	5	49,90	36	58,68	18	85,27	2
S_24	− 1,42	25	9,12	31	60,99	24	75,38	6	85,36	6	98,81	5
S_25	10,08	33	50,74	21	57,98	36	74,97	4	81,59	6	-	-
S_26	− 0,61	3	9,74	14	30,18	18	48,90	34	57,13	19	69,41	12
S_27	9,83	11	47,01	37	47,20	34	58,18	15	73,17	3	–	–
S_28	10,48	2	44,84	30	53,27	57	59,02	11	–	–	–	–
Name	Φ Peak 1	Weight (%)	Φ Peak 2	Weight (%)	Φ Peak 3	Weight (%)	Φ Peak 4	Weight (%)	Φ Peak 5	Weight (%)	Φ Peak 6	Weight (%)
S_02	10,70	19	50,60	66	59,40	14	74,26	1	–	–	–	–
S_29	10,12	5	38,54	14	44,26	14	57,22	66	–	–	–	–
S_30	10,08	2	43,84	73	57,48	19	67,96	5	–	–	–	–
S_32	9,93	15	15,31	3	42,82	43	59,16	27	72,31	11	85,12	1
S_33	3,88	7	10,36	32	57,39	36	62,76	24	85,64	1	99,48	2

Table 3 Comparison of data for fiber orientation distribution of individual samples along polar angle θ. For consecutive peaks in each sample, values of the peak positions' maxima are represented in the first column and their weights are represented in the second column. Weight (%) denotes the ratio of the area of a peak to the area under the kernel fit curve

Name	θ Peak 1	Weight (%)	θ Peak 2	Weight (%)	θ Peak 3	Weight (%)	θ Peak 4	Weight (%)
S_01	87,33	16	90,12	43	90,71	36	95,82	10
S_03	90,13	48	90,80	42	95,58	4	-	-
S_04	80,72	40	90,32	34	95,68	26	-	-
S_05	85,31	42	90,22	32	90,82	16	95,73	10
S_06	83,87	20	90,14	48	92,60	7	96,43	30
S_07	87,01	45	90,35	36	95,95	19	-	-
S_08	86,13	3	90,22	48	92,12	6	96,09	41
Name	θ Peak 1	Weight (%)	θ Peak 2	Weight (%)	θ Peak 3	Weight (%)	θ Peak 4	Weight (%)
S_21	90,16	80	95,16	7	103,45	10	–	–
S_22	87,96	39	90,15	50	95,81	15	–	–
S_23	90,11	28	90,21	45	96,24	25	–	–
S_24	90,36	30	90,47	38	96,28	33	–	–
S_25	90,14	46	91,12	19	95,27	24	96,68	10
S_26	86,87	43	90,20	49	95,75	8	–	–
S_27	90,05	35	90,37	44	95,69	15	–	–
S_28	90,05	49	90,26	42	–	–		
Name	θ Peak 1	Weight (%)	θ Peak 2	W eight(%)	θ Peak 3	Weight (%)	θ Peak 4	Weight (%)
S_02	90,19	74	95,00	15	–	–	–	–
S_29	88,65	35	90,05	32	90,35	32	–	–
S_30	90,03	41	90,25	53	–	–	–	–
S_32	87,83	47	90,24	41	95,72	11	–	–
S_33	90,16	45	91,06	15	95,01	24	96,64	9

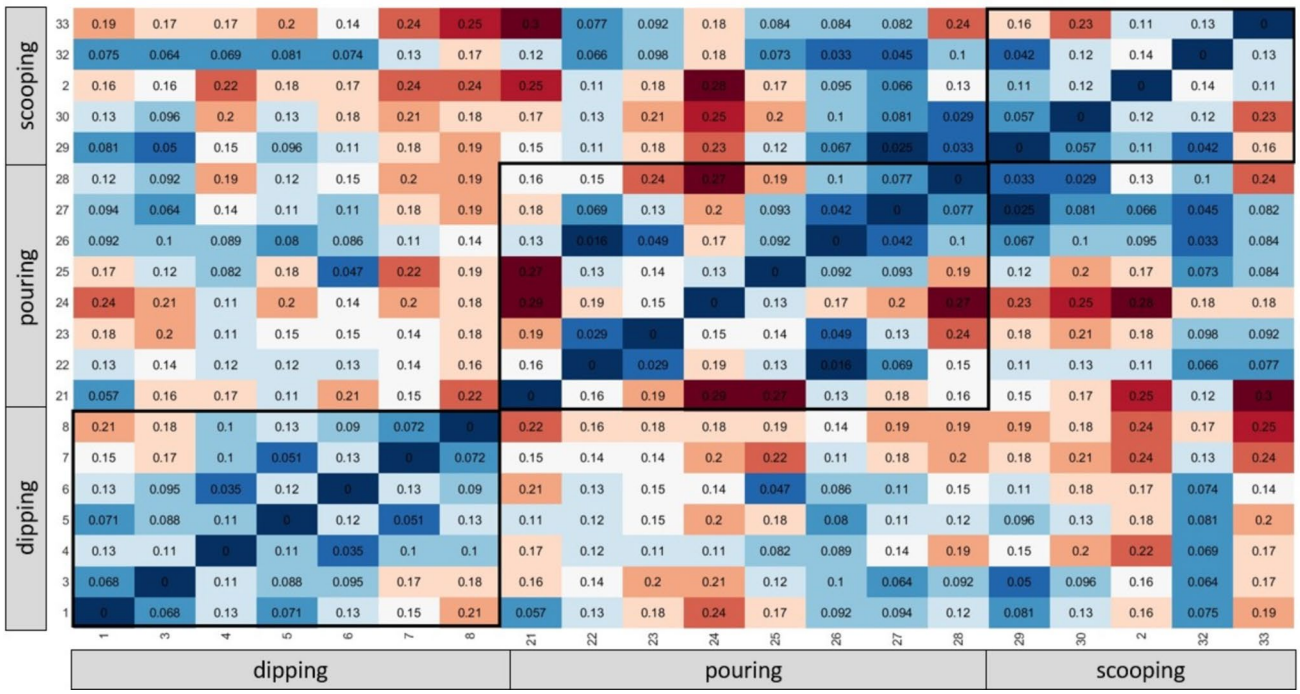

Fig. 11 Heatmap representing the matrix of Jensen—Shannon divergence for the probability distributions of the paper samples along the φ angle

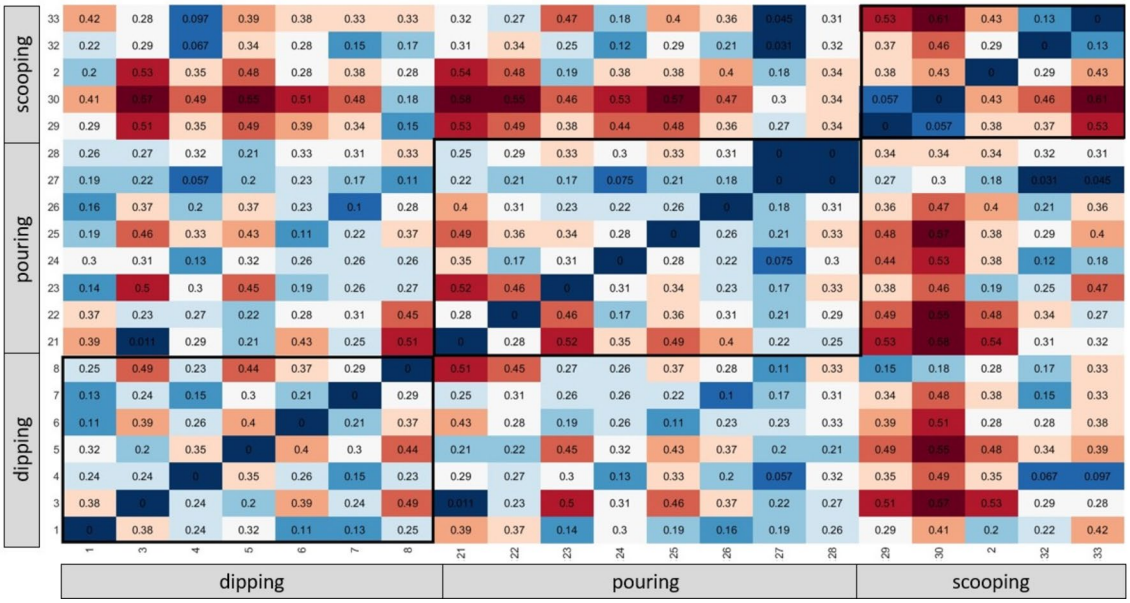

Fig. 12 Heatmap representing the matrix of Jensen—Shannon divergence for the probability distributions of the paper samples along the θ angle

4.2 Fiber orientation

Analysis of the JS divergence matrix suggests that data for orientation along φ angle contains the most valuable information when attempting to differentiate the three sheet formation methods. The majority of fibers in dipped samples appears to be oriented between 40° and 60° φ, as well as below 40° φ, with a notably high contribution of the angle around 10°, being considerably greater than in the other two groups. These numbers suggest a significant role of the gravity force vector in orienting of the fibers in the out-of-plane axis. The presence of modes for higher angle values may be explained by the process of shaking of the mold immediately after lifting it from the vat [https://lecture2go.uni-hamburg.de/l2go/-/get/v/69784]. A skilled papermaker can produce a series of transverse waves within the liquid on top of the sieve, which propagate from the edges of the mold towards the central part of the sieve, counteracting the gravity force of the draining slurry. Because SAXS method provides information on the bulk structure of the material, it does not allow for understanding how does orientation of fibers change with varying depth. It is plausible, however, that in a paper sheet formed by the dipping method majority of the fibers oriented at angles below 40° φ is located in the layers closer to the sieve surface, and that the fibers in the layers further from the sieve experience increasingly less gravity influence and more of the movement in the lateral direction, caused by the waves induced on the surface.

Compared to other groups, samples manufactured by dipping consistently show peaks within the same angle ranges (greatest in-group similarity as measured by JS divergence). For this group of samples, the manufacturing process is well documented with a confirmed consistent way of implementing the dipping method in the sheet formation step. The samples have been produced by single dip method, which is easy to reproduce for consecutive paper sheets, which may explain the high degree of in-group similarity of orientation distribution. Analysis of fiber orientation in-plane by digital microscopy also shows the similarity of orientation distribution across all the samples in this paper group, which further supports a consistent sheet formation method. The low coherency value for this group of samples indicates the distribution of fibers leaning isotropic, which supports the proposed explanation of the processes involved in sheet formation by dipping.

Likely, samples manufactured by pouring show greater variability in orientation distribution, because the fibers are distributed manually on top of the submerged sieve, thus can move freely and assume a certain direction already before the mold is lifted from the vat [https://lecture2go.uni-hamburg.de/l2go/-/get/v/69786]. The greater contribution of peaks for higher φ angle values, above 60° and especially along angles close to 90° suggests stronger influence of the lateral movement during manual distributing of the fibers. This group of samples shows as well a significant contribution of distribution within very low angle ranges, and generally exhibits the greatest average number of modes. These features, as well as lower in-group similarity of distributions compared to the groups of samples manufactured by dipping and scooping, points to possible different types of forces at play in the pouring method. Apart from distribution of the slurry by hand which consists in stirring the fibers by

circular movements, for this group of samples no formation aids were used in their production, so the possibility of turbulent flow arises locally, which might cause the non-uniform distribution of fibers and their flocculation. It is plausible as well, that the role of fiber-to-fiber interaction is non-negligible, as this method involves more concentrated slurry.

For the group of samples manufactured by scooping, the significantly greater contribution of peaks for φ angle values between 40° and 60°, when compared to two other sheet formation methods, could be linked to the fact that in scooping, the gravity force is counterbalanced by the laminar flow of the slurry distributed on top of the sieve [https://lecture2go.uni-hamburg.de/l2go/-/get/v/69788]. This method of sheet formation involves as well depositing of a much smaller amount of the slurry on the sieve. When compared to the dipping method, where the sieve is dipped deeper in the vat and greater force of a larger mass of water is excreted on the fibers during draining, it seems plausible that in the scooping method less fibers is directed out-of-plane of the paper sheet. Greater in-group similarity for the group of scooped samples was expected, but their exact manufacturing parameters are not known. Traditionally, different variants of the scooping method are practiced, which could involve movement in the direction forward from the papermaker, as well as to the sides. The results of fiber orientation imaging in plane of the paper sheet reveal that the dominant orientation angle within this group is variable with most of the samples exhibiting fiber orientation in the direction forward from the papermaker (80–90°) or to the sides (0–10°). The high side-specific average coherence value for scooped papers group suggests higher in-plane fiber orientation anisotropy, which may result from the drag of fibers in the direction of the laminar flow induced in this sheet formation technique.

At the present, early stage of the project we are aware of certain limitations of the proposed approach. The number of samples measured thus far is relatively small, which means that with adding more samples we might discover that the measurement and data analysis protocol in the current form are insufficient. The Gaussian Mixture Model fitting strategy is exploratory and somewhat arbitrary, as we are assuming that the orientation distributions are built of a certain number of multiple true normal distributions, which may appear to be an overly simplistic approach when populating the database with samples exhibiting more technological variability. We predict that together with increasing complexity of the sample set we will need to derive a machine learning model, which may include, but certainly not remain limited to, the steps and algorithms proposed in this study. Factors that could increase the difficulty of interpretation may be multiple, such as the relationship of fiber orientation and distribution to the type of raw material, which cannot be fully understood based on the current results. In the case of historical papermaking technologies, there is a strong correlation between material type and the types of processes involved; certain plant fiber species were used only in particular sheet formation methods with appropriate additives. An example of such an established relationship is the use of Asian bast fibers and natural mucilages in the scooping sheet formation technique. In the following stages of the project, the influence of particular ingredients and papermaking parameters on fiber distribution will be explored by means of a designed experiment, which should allow for more in-depth analysis.

Author contributions MG: conceptualization, methodology, data analysis, writing, reviewing, SH: conceptualization, methodology, writing, data analysis, reviewing. AHW: project administration, conceptualization, methodology, reviewing.

Funding Open Access funding enabled and organized by Projekt DEAL.

Data availability The data sets generated and/or analyzed during the current study are available from the corresponding author upon reasonable request.

Declarations

Conflict of interest No potential conflict of interest was reported by the authors.

Bibliography:s

1. M. Korstschot, The role of the fibre in the structural hierarchy of paper. In The Fundamentals of Papermaking Materials, Trans. of the XIth Fund. Res. Symp. Cambridge, 1997, ed. By C.F. Baker, 351–399 (FRC, Manchester, 2018)
2. F.R. Santos, J.C. Lopes Ribeiro, J.M. de Carvahlo, W.L. Magalhaes, L.G. Pedroti, G.N. Nalon, G.E. Soares de Lima, Nanofibrillated cellulose and its applications in cement-based composites: a review. Const. Build. Mater. (2021). https://doi.org/10.1016/j.conbuildmat.2021.123122
3. G. Chinga Carassco, Cellulose fibers, nanofibrils and microfibrils: the morphological sequence of MFC components from a plant physiology and fibre technology point of view. Nano. Res. Let. (2011). https://doi.org/10.1186/1556-276x-6-417

4. M. Sfiligoj Smole, S. Hribernik, S. Kleinschek, T. Kreze, T., Plant fibers for textile and technical applications, in *Advances in Agrophysical Research*. ed. by S. Grundas (A. Stepniewski, 2012)
5. L.J. Gibson, The hierarchical structure and mechanics of plant materials. J. R. Soc. Interface. **9**(76), 2749–2766 (2012). https://doi.org/10.1098/rsif.2012.0341
6. M. Konigsberger, M. Lukacevic, J. Fussl, Multiscale micromechanics modeling of plant fibers: upscaling of stiffness and elastic limits from cellulose nanofibrils to technical fibers. Mater. Struct. (2023). https://doi.org/10.1617/s11527-022-02097-2
7. M. Ilvessalo-Pfäffli, *Fiber Atlas* (Springer, Berlin, 1995)
8. J. Trier. (2022). Ancient Paper of Nepal. Result of Ethnotechnological Field Work on its Manufacture, Uses and History with Technical Analyses of Bast, Paper and Manuscripts (Jutland Archaeological Society Publications, Copenhagen, 1972)
9. T. Mahmood, A. Kamal, Ash properties relevance to beneficial uses. Waste Manage. (2022). https://doi.org/10.1016/j.wasman.2021.11.018
10. P. Przybysz, M. Dubowik, M.A. Kucner, K. Przybysz, K. Przybysz Buzała, Contribution of hydrogen bonds to paper strength properties. PLoS ONE (2016). https://doi.org/10.1371/journal.pone.0155809
11. K. Nyholm, P. Ander, S. Bardage, G. Daniel, Dislocations in pulp fibers – their origin, characteristics and importance – a review. Nord. Pulp Pap. Res. J. **4**(16), 376–384 (2001). https://doi.org/10.3183/npprj-2001-16-04-p376-384
12. R.J. Kerekes, C.J. Schell, Effects of fiber length and coarseness on pulp flocculation. Tappi J. **78**(3), 133–146 (1995)
13. H. Yan, T. Lindstrom, M. Ankerfors, Fibre length effect on fibre suspension flocculation and sheet formation. Nordic Pulp Paper Res. J. **21**(1), 30–35 (2006). https://doi.org/10.3183/npprj-2006-21-01-p030-035
14. R. J. Kerekes, Perspectives on fibre flocculation in papermaking. International Paper Physics Conference. In 1995 Proceedings of the International Paper Physics Conference, CPPA, Montreal, 23–31 (1995)
15. P. Larsson, T. Lindström, L.A. Carlsson, C. Fellers, Fiber length and bonding effects on tensile strength and toughness of kraft paper. J. Mater. Sci. **53**, 3006–3015 (2017). https://doi.org/10.1007/s10853-017-1683-4
16. H. Lindqvist, K. Salminen, J. Kataja-aho, E. Retulainen, P. Fardim, A. Sundberg, The effect of fibre properties, fines content and surfactant addition on dewatering, wet and dry web properties. Nordic Pulp Paper Res. J. (2012). https://doi.org/10.3183/npprj-2012-27-01-p104-11
17. B. Sjöstrand, R. Deshpande, M. Thyrel, G. Henriksson, Dewatering properties of pulps made from different parts of a Norway spruce (Picea abies). Nord. Pulp Pap. Res. J. **37**(4), 702–711 (2022). https://doi.org/10.1515/npprj-2022-0050
18. R.J.N. Helmer, G.H. Covey, W.D. Raverty, N. Vanderhoek, G. Tan, Forming fabrics, drainage rates and paper properties. Appita Techn Inn Manuf Environ. **56**(4), 202–206 (2002)
19. M.A. Hubbe, J.A. Heitmann, Review of factors affecting the release of water from cellulosic fibers during paper manufacture. BioResources (2007). https://doi.org/10.15376/biores.2.4.500-533
20. H. Yum, History and function of dispersion aids used in traditional East Asian papermaking. J. Inst. Con. (2011). https://doi.org/10.1080/19455224.2011.607008
21. J.F. Waterhouse, Effect of papermaking variables on formation. Tappi J. **76**(9), 129–134 (1993)
22. R. Holm. 2004. Fluid mechanics of fibre suspensions related to papermaking. Doctoral Thesis. (Royal Institute of Technology, Stockholm, Sweden)
23. A. Svedberg, Improvement of the retention – formation relationship using three – component retention aid systems, Doctoral Thesis, (Royal Institute of Technology, Stokholm, Sweden, 2012) 24. H. Cui, J. R. Grace, Flow of pulp fiber suspensions and slurries: A review. International Journal of Mutliphase Flow. **33**, 921–934. (2007). https://doi.org/10.1016/j.ijmultiphaseflow.2007.03.004.
24. F. Lundell, F. D. Soderberg, P. H. Alfredsson, Fluid Mechanics of Papermaking, Annual Reviews in Fluid Mechanics, 43, 195–217 (2011), https:// 2011. 43:195–217
25. A. Helman-Ważnym, C. Ramble, The Mustang Archives: Analysis of handwritten documents via the study of papermaking traditions in Nepal, (Turnhout: Brepols, monograph in the Silk Road Studies series), 182–187 (2021)
26. A. Helman-Ważny, 23 The Choice of Materials in Early Tibetan Printed Books, In Tibetan Printing: Comparisons, Continuities and Change, ed. By H. Diemberger, F. Ehrhard, P. Kornicki, Leiden, (Brill, The Netherlands, 2016), 532 – 554 https://doi.org/10.1163/9789004316256
27. T. Enomae, Y.H. Han, A. Isogai, Nondestructive determination of fiber orientation distribution of paper surface by image analysis. Nord. Pulp Pap. Res. J. **21**(2), 253–258 (2006). https://doi.org/10.3183/NPPRJ-2006-21-02-p253-259
28. T. Enomae, Y.H. Han, A. Isogai, Z-Directional distribution of fiber orientation of Japanese and western papers determined by confocal laser scanning microscopy. J. Pulp Pap. Sci. **33**(2), 100–105 (2008). https://doi.org/10.1007/s10086-008-0950-z
29. C. Bergfjord, H. Bodil, A procedure for identifying textile bast fibres using microscopy: flax, nettle/ramie. Hemp. Jute. Ultramicro. **110**(9), 1192–1197 (2010). https://doi.org/10.1016/j.ultramic.2010.04.014
30. H. Lukesova, H. Bodil, Identifying plant fibres in cultural heritage with optical and electron microscopy: how to present results and avoid pitfalls. Her. Sci. (2024). https://doi.org/10.1186/s40494-023-01122-z
31. M. El Boustani, F. Brouillette, G. Lebrun, A. Belfkira, Solvent-free acetylation of lignocellulosic fibers at room temperature: effect on fiber structure and surface properties. J. Appl. Polym. Sci. (2015). https://doi.org/10.1002/app.42247
32. F. Saxe, M. Eder, G. Benecke, B. Aichmayer, P. Fratzl, I. Burgert, M. Rüggeberg, Measuring the distribution of cellulose microfibril angles in primary cell walls by small angle X-Ray scattering. Plant Methods (2014). https://doi.org/10.1186/1746-4811-10-25
33. Püspöki, Zsuzsanna, Martin Storath, Daniel Sage, and Michael Unser. "Transforms and Operators for Directional Bioimage Analysis: A Survey." In Focus on Bio-Image Informatics, edited by Winnok H. De Vos, Sebastian Munck, and Jean-Pierre Timmermans, 219:69–93. Advances in Anatomy, Embryology and Cell Biology. Cham: Springer International Publishing,.
34. S. Haas, X. Sun, A.L.C. Conceicao, J. Horbach, S. Pfeffer, The new small-angle X-ray scattering beamline for materials research at PETRA III: SAXSMAT beamline P62. J. Synchrotron Rad **30**(6), 1156–1167 (2023). https://doi.org/10.1107/S1600577523008603
35. A. Gimat, S. Schöder, M. Thoury, A.L. Dupont, Degradation of historical paper induced by synchrotron X-ray technical examination. Cellulose **29**(8), 4347–4364 (2022). https://doi.org/10.1007/s10570-022-04552-3
36. G. Ashiotis, A. Deschildre, Z. Nawaz, J.P. Wright, D. Karkoulis, F.E. Picca, J. Kieffer, The fast azimuthal integration Python library: pyFAI. J. Appl. Crystallogr. **48**, 510–519 (2015). https://doi.org/10.1107/s1600576715004306
37. M. Georgiadis, M. Guizar-Sicairos, A. Zwahlen, A.J. Trüssel, O. Bunk, R. Müller, P. Schneider, 3D scanning SAXS: A novel method for the assessment of bone ultrastructure orientation. Bone (2015). https://doi.org/10.1016/j.bone.2014.10.002